to appear in ApJL.

Limitation of the pupil replication technique in the presence of instrumental defects

P. Riaud[1], D. Mawet[1], O. Absil[1]

Institut d'Astrophysique et de Géophysique de Liège, 17 Allée du 6 Août, Bât B5c, B-4000 Liège, Belgium

riaud@astro.ulg.ac.be, mawet@astro.ulg.ac.be, absil@astro.ulg.ac.be

ABSTRACT

Pupil replication has been proposed by Greenaway et al. 2005 as a new optical technique to improve the suppression of starlight in high dynamic imaging. This paper extends numerical simulations in the two-dimensional case with various realistic imperfections (surface error, chromatic smearing and pupil shift). These results demonstrate some strong limitations compared to single pupil apodization techniques for exoplanet detection.

Subject headings: planetary systems — stars: imaging — techniques: high angular resolution

1. Introduction

The main problem in exoplanet search is the contrast between the host star and its potential exoplanets. For an Earth-like planet, the flux ratio is 10^{10} in the visible and 10^6 in the thermal infrared around $10\,\mu m$. Generally, the star halo strongly contaminates planetary images. The Airy rings can be attenuated by appropriate pupil apodization techniques (Aime et al. 2002) for example. But far away (beyond $10\lambda/d$, with d the telescope diameter), the ultimate speckle level limits the detectability of faint sources such as exoplanets. Greenaway et al. (2005) have recently presented a new technique called "Pupil replication" (Greenaway et al. 2005) (GR05 hereafter) to decrease the diameter of the star image in the

[1]Post-doc Astronomer, under PAI contract.

focal plane. This technique transforms a simple telescope into a pseudo-interferometer by juxtaposing a number of replica of the initial pupil. Therefore, the field of view properties are analogue to the pupil densification technique (Labeyrie 1996; Pedretti et al. 2000; Riaud et al. 2002; Gillet et al. 2003). A classical apodization scheme (super-Gaussian) is presented in GR05 to achieve adequate suppression of the stellar halo. In this paper, unlike in GR05 where all simulations are one-dimensional, we study the optical properties for two-dimensional systems with the following consequences: classical circular apertures do not appear optimal for the pupil replication technique; only pupil shapes like squares or hexagons can be used to achieve optimal extinction effects. Moreover, the two-dimensional simulations clearly show a dispersion of the planetary flux, not only in the radial direction as in one-dimensional images, but across the whole image plane (Figure 3). The associated flux losses are thus larger than the ones observed in the one-dimensional simulations in the paper GR05. Then, we discuss the effect of surface errors due to polishing defects in the optical workbench. Finally, the most severe source of performance degradation seems to be the possible misalignment between the sub-pupils, whereas pointing errors result in only weak losses. This article explains and quantifies these principal limitations of the pupil replication technique for exoplanet search.

2. Simulation results

2.1. Basic results

We have performed two-dimensional numerical simulations of pupil replication in conditions close to the ones used in GR05. The replication system consists of 3×3 pupils arranged on a square. With this configuration, the core of the star is three times narrower in the X,Y-directions than in the single pupil case. In our simulations, all images (replicated and not replicated) correspond to a sum of twenty elementary images at different wavelengths with the appropriate (super-Gaussian) apodization technique in the considered bandpass (760 to 1000 nm, like in GR05). All angular separations will be given with respect to the central wavelength of 880 nm and we will consider that the replication scheme is perfect in term of transmission (ideal beam splitters). In the two-dimensional case, the optical efficiency of the system is $\approx 41\%$ for square pupils instead of 65% in 1D. This difference is simply due to the conservation of energy (each replica possess 1/9 of the total energy) and the two-dimensional geometry integration: the apodization profile must be azimuthally integrated on the 3×3 replicated pupil, which leads to a very poor transmission for the four replica at the corners of the scheme.

Three possible configurations can be considered, with circular, square or hexagonal sub-

pupils. The first configuration (circular), although the most common, is unfortunately not optimized for a best rejection factor due to the gaps between replicated pupils. The last two configurations (square and hexagonal) produce a replicated arrangement without gaps, thus optimized for high contrast imaging. In the following study, we will therefore focus on the square-pupil geometry with the super-Gaussian apodization. It must be noticed that ASA apodization (Nisenson & Papaliolos 2001) appears to be the best for square-pupil geometry but unfortunately is also the more difficult to manufacture. The chosen apodization (super-Gaussian) is centro-symetric in order to have a full working angle, and to provide a direct comparison with GR05.

The first simulations consist in comparing the results in the one- and two-dimensional cases (the latter not being considered in GR05). With the square geometry, the best result in the residual level is 10^{-14} of the central star flux. We will see it in the following section that this level is critically dependent on the wavefront bumpiness and pupil misalignments. Figure 1 compares the replicated apodized case with a single apodized pupil. The numerical simulations are performed with a low wavefront error ($\lambda/2500$ rms @ 632.8 nm) and in polychromatic light (760 to 1000 nm).

2.2. Performance estimation for a real system

Now, let us investigate three important limitations of the pupil replication technique. First, the wavefront bumpiness of both the telescope and optical replication scheme is considered. Indeed, we have so far presented the basic results with ultimate optics characteristics ($\lambda/2500$ rms @ 632.8 nm). Figure 2 shows the results obtained with various wavefront errors between $\lambda/30$ and $\lambda/2500$ rms. To simplify the analysis, we have supposed that the wavefront bumpiness of the replication scheme is the same as for the telescope, which might reveal to be optimistic (the beam splitters will not be perfect). Thus all wavefront errors mentioned in this article should be multiplied by $\sqrt{2}$ to have the global wavefront error. In Figure 2, we clearly see an important gain for wavefront errors smaller than $\lambda/250$ rms.
This result is interesting in terms of feasibility. Indeed, the Virgo team (Mackowski et al. 1999; Brillet et al. 2003) has demonstrated state-of-the-art mirror quality with excellent polishing realization ($\lambda/226$ rms @ 632.8 nm), within the framework of gravitational wave detection. This technology is directly applicable for Bracewell nulling interferometers (Bracewell & McPhie 1979), apodization and coronagraphy (Baudoz et al. 2000; Riaud et al. 2003). Other applications such as EUV lithography process also need excellent mirror quality. Let us cite for example the realization of small EUV mirrors with a wavefront error around $\lambda/1800$ rms @ 632.8 nm (Goldberg et al. 2002). The first value given by the Virgo team seems to be realistic

although somewhat pessimistic in the sense that further developments may improve this figure. A $\lambda/250$ rms wavefront bumpiness seems to be a reasonable goal.

The second limitation of pupil replication for high contrast imaging is the flux attenuation of an off-axis source. The pupil replication can be seen as a pseudo-interferometer creating multiple dispersed peaks referred to as "chromatic smearing" in GR05. The calculated flux attenuation of an off-axis source in 4 resolution elements, i.e. $(2.\lambda/d)^2$, is an oscillating function. Figure 3 shows numerical simulations of off-axis sources in the case of $\lambda/2500$ rms wavefront bumpiness. The mean attenuation factor is 42% with respect to the on-axis source. The attenuation in the case of $(3.\lambda/d)^2$ and $(\lambda/d)^2$ becomes 36% and 64% respectively.

A third important limitation of the new technique is the sensitivity to the relative positioning of the different replicated pupils. As already seen in Figure 1, in which case the pupils are not perfectly joined because of their circular shape, the starlight residuals for large angular separations can be as high as 10^{-6}. In the case of pupil misalignments, this effect can become even more important. Indeed if the pupil arrangement presents some gaps, the system behaves like a Fizeau interferometer and creates a large number of dispersed peaks. The large bandwidth and the scattering effect due to wavefront bumpiness give an even increased starlight level. Figure 4 shows a loss in starlight rejection as large as 7 orders of magnitude for angular separations larger than $3\lambda/d$ with respect to the ideal case of Figure 1, when the pupils are misaligned by 0.5% or more. A detailed analysis, including the effects of the Fresnel diffraction between the edges of the pupils (an oscillating function), shows a clear improvement of the system performance for pupil misalignments smaller than 0.1%. However, assuming a 1 cm replicated pupil size, a good alignment with a 10 μm precision still induces a loss of 6 orders of magnitude in starlight rejection.

Finally, the last effect on the residue level is the pointing jitter. Indeed, pupil replication consists in artificially increasing the angular resolution like a pseudo-interferometer. Small jitter errors induce a relatively small effect compared to pupil misalignment with a degradation ranging from a factor 4 to 6 on the whole angular domain for jitter errors between 1 and 15 mas rms.
Taking all errors into account, the gain is in fact larger than 1 only for short angular separations ($< 3\lambda/d$) and does not exceed around 5 in the application range where the replication technique would be interesting (1-18 λ/d, see Figure 1), as illustrated in Figure 5. Let us emphasize that we have chosen perfect beam splitters in these simulations. With state-of-the-art commercial components ($\lambda/100$ rms at 632.8 nm and an amplitude mismatch of 5%),

the total wavefront bumpiness would amount to $\lambda/60$ rms and the nominal performance of the system would not be achieved. A new instrumental approach is thus necessary.

3. Discussion and perspectives

We have demonstrated several important limitations of the pupil replication technique presented by Greenaway et al. 2005. Originally, this technique was presented in the one-dimensional case. Our numerical analysis for the two-dimensional case shows new effects like diffraction between adjacent sub-pupils due to pupils misalignment that strongly affect the efficiency of this technique.

In the case of Extreme Adaptive Optics implementation on ground-based telescopes or high contrast imaging on space telescopes, a classical Lyot coronagraph or a phase-mask coronagraph gives the same or better performances than this technique with much simpler implementation while preventing the saturation behaviour.

Pupil replication technique must be used in complement of other apodization or nulling schemes, but not alone. It seems to be more appropriate to use this technique after a coronagraphic mask, or more precisely, after the coronagraphic diaphragm that blocks most of the starlight. Doing so, we relax important limitations like wavefront bumpiness and pupil shear. The starlight diffusion induced by the wavefront defects of the replication scheme can be overcome by attenuating its main contribution upstream with a pre-coronagraphic stage. Thanks to the coronagraphic attenuation, the tolerance on the wavefront bumpiness is consequently relaxed at about $\lambda/4$ PTV. Moreover, the upstream starlight attenuation and the absence of apodization now allows to use circular pupils without producing a too large amount of spurious starlight in the following image plane. We propose to take advantage of these properties by using a three stage optical implementation as shown in Figure 6): the first stage consists in a phase mask coronagraph (quasi-achromatic 4QZOG, Mawet et al. 2005), followed by a 3×3 pupil replication scheme for classical circular pupils. In the following interferometric image plane and as a third stage we place a simple Lyot coronagraph (dark spot) followed by its diaphragm to further enhance the contrast. K-band preliminary numerical simulations show a gain of ≈ 40 on the stellar peak attenuation with respect to the 4QZOG alone (Mawet et al. 2005), with a null depth of 4.5×10^{-7}. In this simulation, we take into account realistic wavefront errors both for the telescope ($\lambda/250$ rms) and the pupil replication scheme ($\lambda/50$ rms) with respect the central wavelength 2.2 μm (see Figure 7). Nevertheless, given the optical complexity, such a multi-stage scheme should be experimented on a coronagraphic workbench in order to prove its relevence and assess the real gain that it could provide.

We are grateful for the referee A. Greenaway, and F.H.P. Spaan for useful discussions and suggestions especially concerning chromatic smearing. The first author also acknowledges the financial support of the Belgian fund "Pôle d'Attraction Inter-universitaire (IAP)".

REFERENCES

Aime, C., Soummer, R. & Ferrari A. 2002, A&A, 389, 334

Baudoz, P. et al. 2000,A&AS, 141, 319

Brillet A. et al. 2003,Phys. Rev. D, 67, 102006

Bracewell, R.N. & McPhie, R.H. 1979, Nature, 274, 780

Gillet, S. et al. 2003, A&A, 400, 396

Goldberg K.A. et al. 2002, J. Vac. Sci Technol. B, 20(6), 2834

Greenaway, A.H., Spaan, F.H.P. & Mourai V. 2005, ApJ, 618, L165

Labeyrie, A. 1996, A&A, 118,517

Mackowski, J.M. et al. 1999, Opt. & Quant Elect., 31 (5-7), 507

Mawet, D. et al. 2005, to appear in Appl. Opt.

Nisenson, P. & Papaliolos, C. 2001, ApJ, 548, L201

Pedretti, E. et al. 2000, A&AS, 147, 285

Riaud, P. et al. 2002, A&A, 396, 345

Riaud, P. et al. 2003, PASP, 115, 712

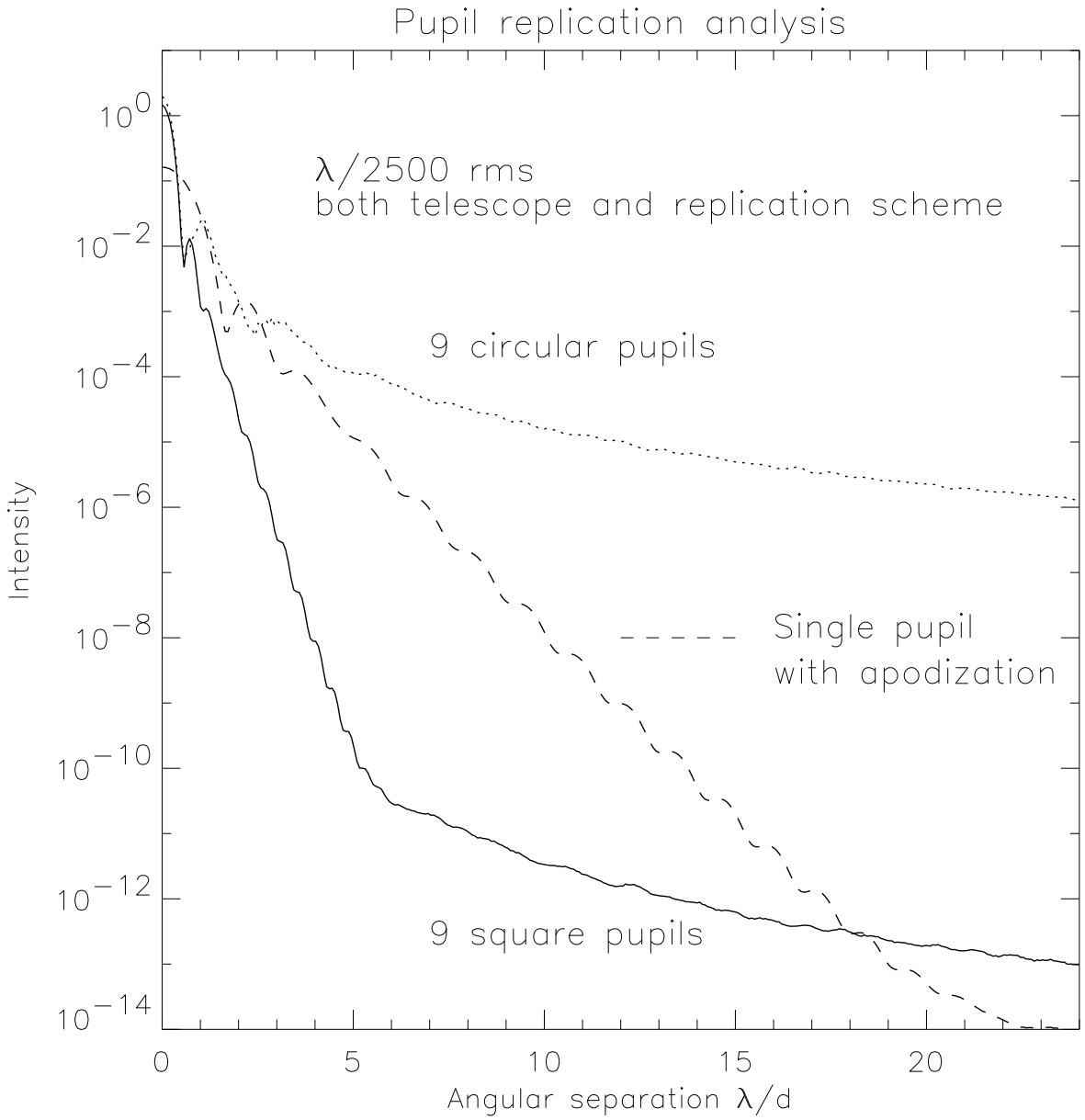

Fig. 1.— Numerical simulations illustrating the effect of replication on the square pupil. The solid line shows the starlight level as a function of angular distance in the case of the super-Gaussian apodization for the two dimensionnal replicated scheme (9 replicated pupils). The dotted line shows the case of a two dimensionnal replicated scheme with 9 circular pupils. The dashed line illustrates the apodization effect on a single pupil. All simulations are performed in polychromatic (760 to 1000 nm) and low wavefront error ($\lambda/2500$ rms @ 632.8 nm). The effect of the replication technique on the star level is clearly visible: only the domain between 1 and 18 λ/d presents a possible gain with a square entrance pupil for high contrast imaging. The classical circular entrance pupil presents less interest.

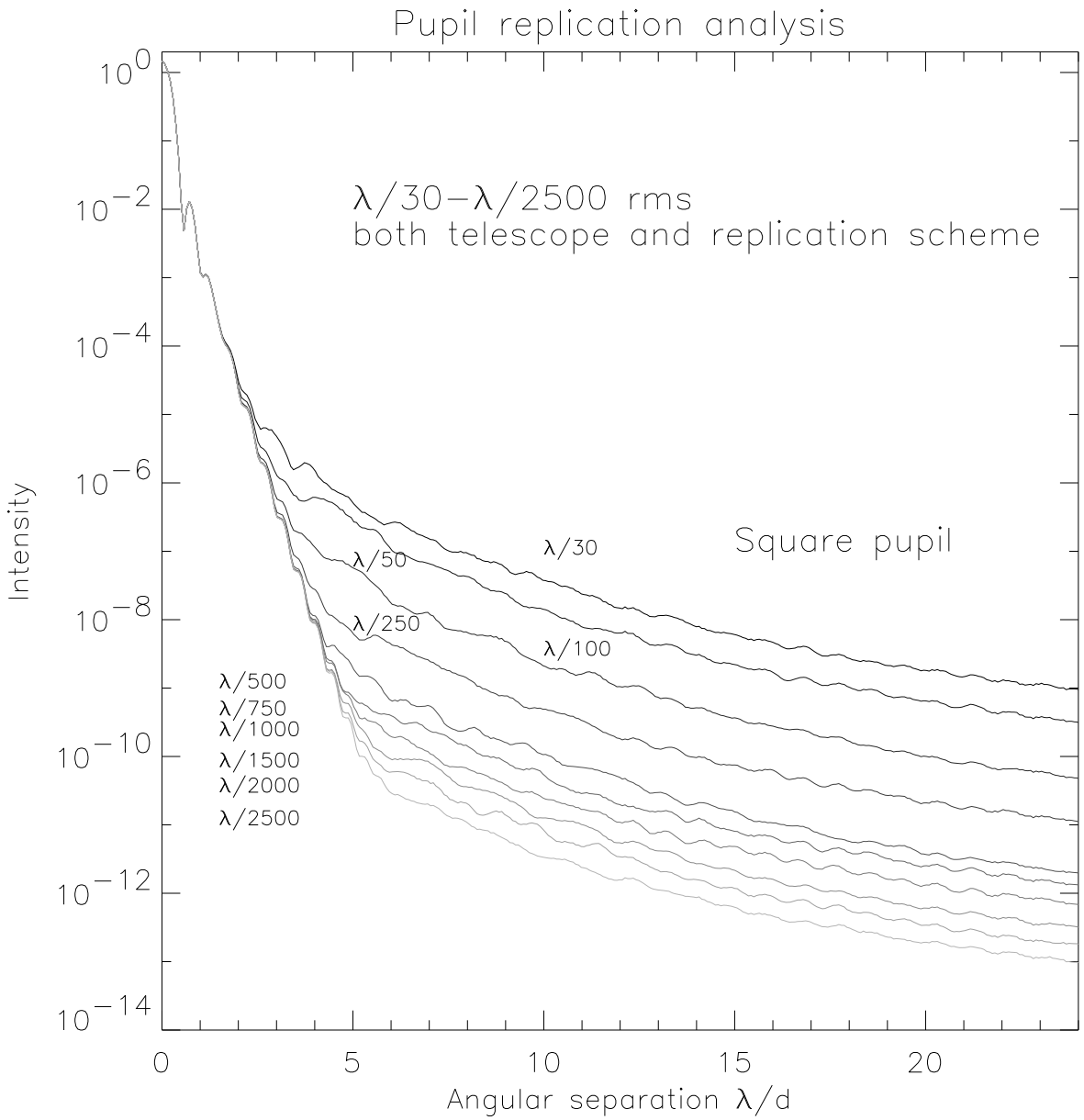

Fig. 2.— Simulated radial profiles for square pupil replication in presence of polishing errors. We present the starlight level for various wavefront errors between $\lambda/30$ to $\lambda/2500$ rms for both the telescope and replication optics. The simulations show an important gain for wavefront errors smaller than $\lambda/250$ rms.

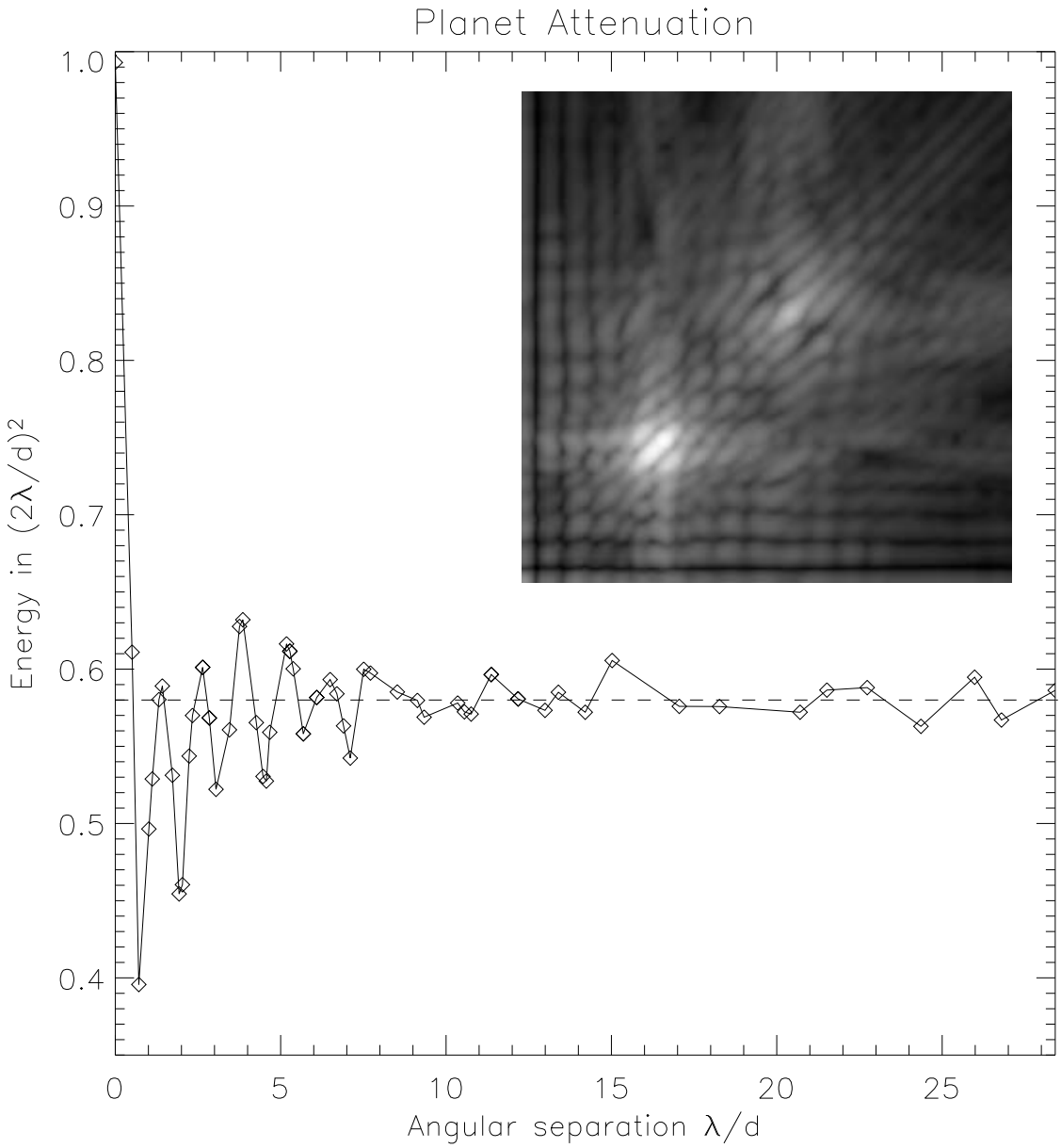

Fig. 3.— Numerical simulations of chromatic smearing of a planetary peak. An off-axis planetary peak spreads out on a large surface, thereby inducing a dilution of flux. We calculate the flux of an off-axis point-like source in 4 resolution elements centered around the maximum of the intensity. We demonstrate here a flux loss depending on the angular separation. We show large oscillations for angular separations smaller than $10\lambda/d$, and then a quasi-constant loss of 42% further out. The image shows the reponse of the replication system in logarithmic scale for an off-axis planet ($4\lambda/d$) with the lower left corner being on-axis.

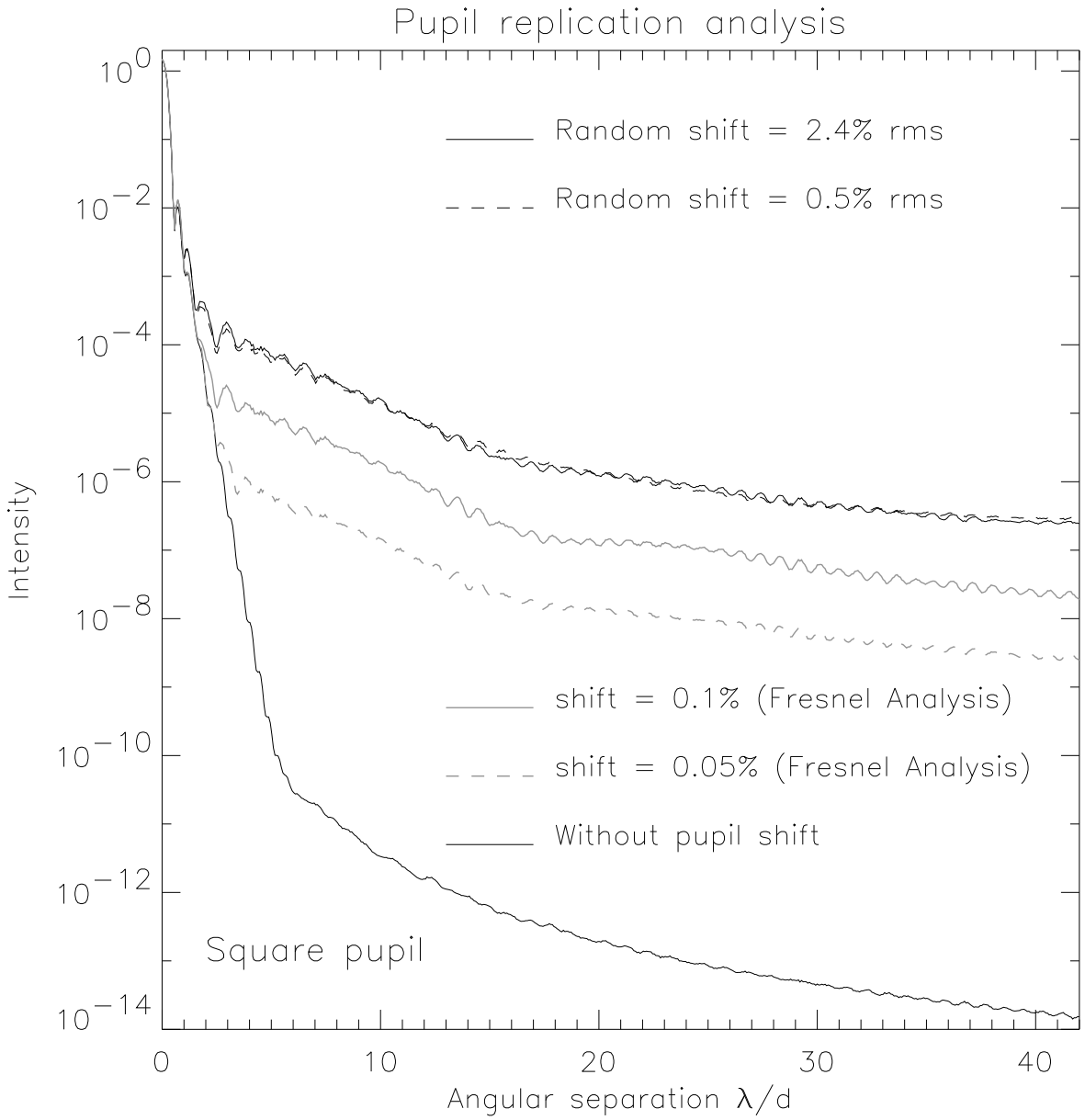

Fig. 4.— Simulated effect of pupil misalignment in the replication optical scheme. A 0.5% rms already gives an important loss of about 7 orders of magnitude for angular separations larger than $3\lambda/d$. The curve at 0.5% present only small variations with respect to the first one (2.4%). This relates to the fact that the presence of gaps induces high diffraction residues in the final images. A Fresnel diffraction analysis (0.1% and 0.05% pupil mislignment) shows a signifiant improvement in stellar rejection by a factor 10 and 100 respectively. Assuming a 1 cm replicated pupil, these misalignments respectively correspond to 240, 50, 10 and 5 μm. A 10μm alignment precision is currently state-of-the-art. The gap between each replica should be smaller than 2 μm to achieve a 10^{-10} level of contrast at 40 λ/d.

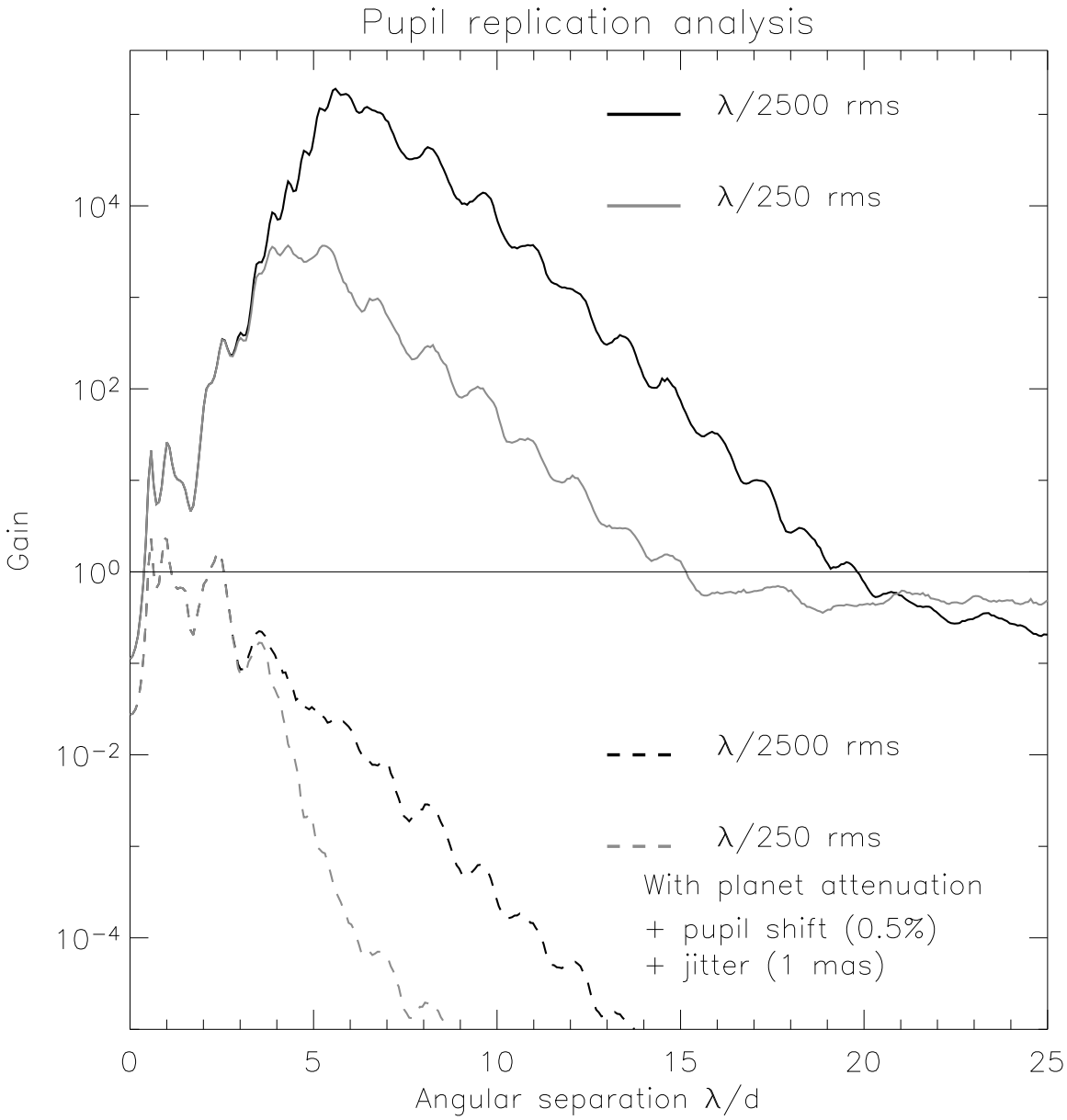

Fig. 5.— Numerical simulations of the gain in starlight level between the apodized and replicated scheme and the simple pupil apodization. These simulations are given for two possible wavefront bumpinesses ($\lambda/250$ rms in grey and $\lambda/2500$ rms in black). The two solid curves illustrate the gain provided by this technique without instrumental defects other that wavefront errors, while the two dashed curves correspond the same numerical simulations taking into account flux loss for an off-axis source (see Fig. 3), a pupil misalignment of 0.5% (see Fig. 4) and a 1 mas jitter. All profiles are azimuthally averaged. This simulation shows a poor gain (≤ 5) for short angular separations ($< 3\lambda/d$). With a pupil alignment around 0.1% , the gain would range from 5 to 40 for angular separation lower than $< 4\lambda/d$.

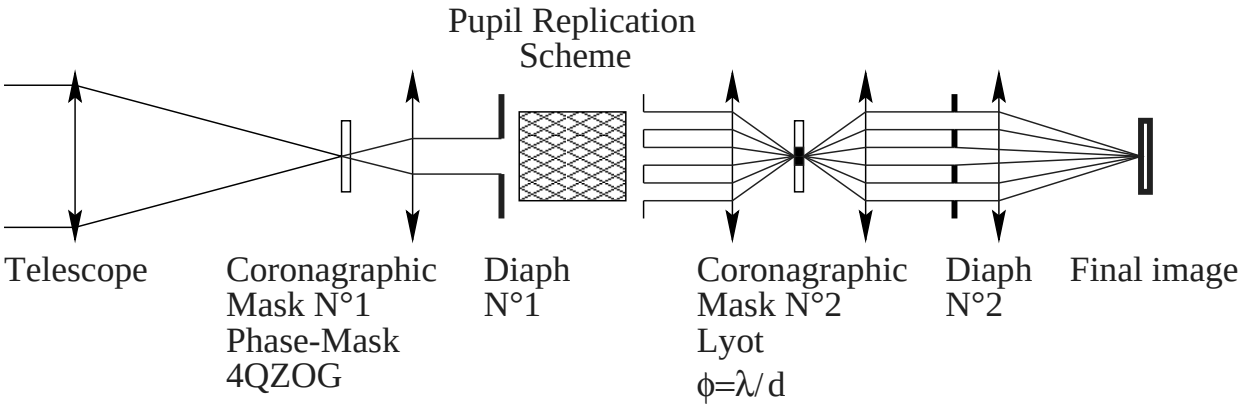

Fig. 6.— Example of multi-stage coronagraphic implementation of the pupil replication scheme. The first stage consists of a phase-mask coronagraph like the 4QZOG that allows full Inner Working Angle. The first diaphragm removes most of the starlight contribution, but even if after it, a central peak due to tip-tilt errors and chromatism still remains in the coronagraphic image. As a second stage, the replication scheme creates nine circular replicated pupils. This configuration forces the stellar peak residue to shrink in the pseudo-interferometric image. In this image plane, we use as a third stage a second coronagraphic mask: a simple Lyot with a diameter of only λ/d instead of $6\lambda/d$ in the classical approach of single-pupil coronagraphy. The Lyot mask removes the narrower stellar peak and improves the detectability in the final image by a factor of about 40.

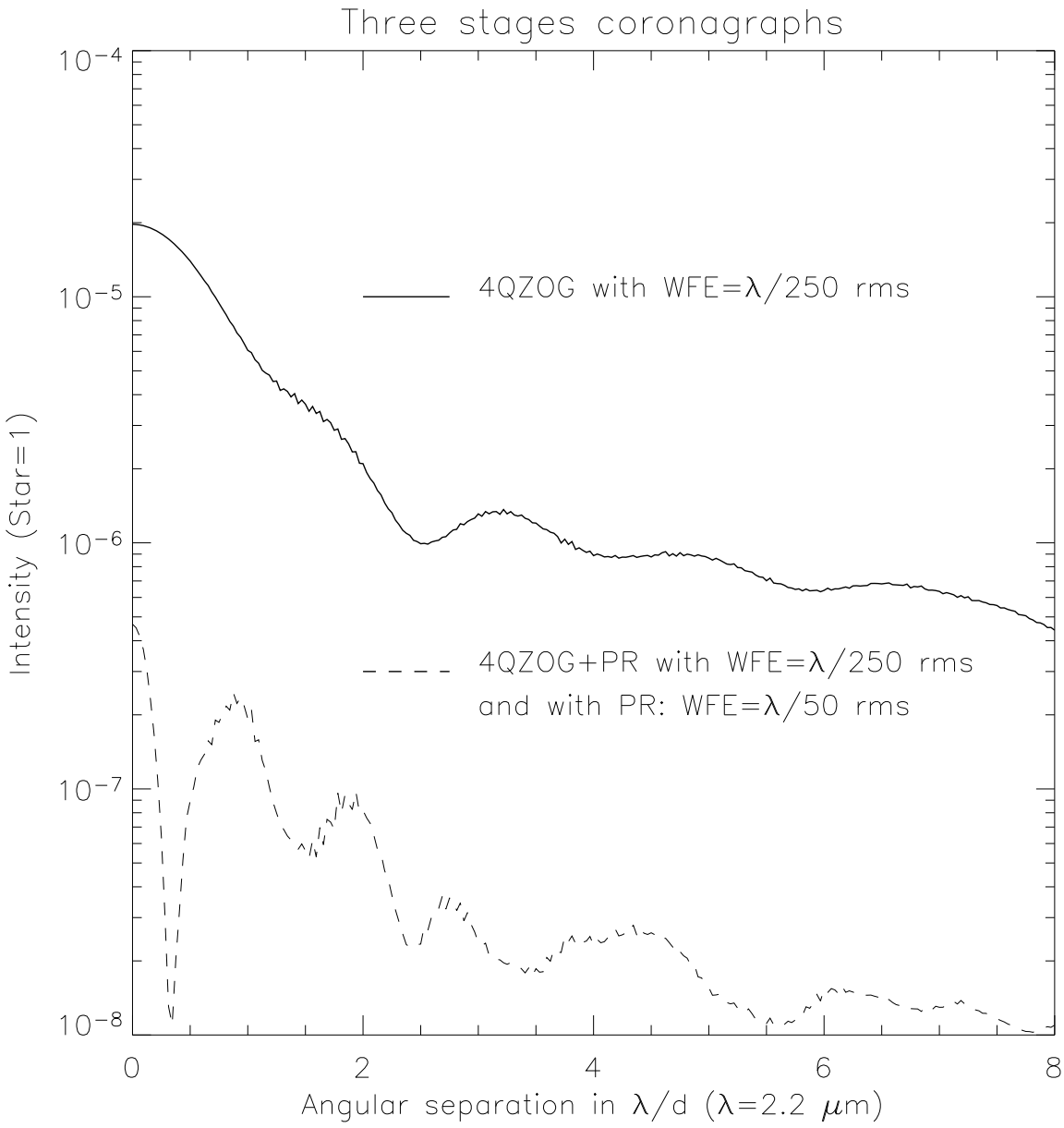

Fig. 7.— Numerical simulation results for a multi-stage coronagraph. The first coronagraph is the quasi-achromatic 4QZOG (Mawet et al. 2005). The null depth with respect to the star is around 2×10^{-5} with a wavefront errors on the entrance pupil of $\lambda/250$ rms. A second coronagraphic mask, a simple Lyot with a diameter of only λ/d, placed after a pupil replication device, gives a gain in the central stellar peak in the final image of ≈ 40. It must be noted that the wavefront errors of the replication scheme (PR) is strongly relaxed here with only $\lambda/50$ rms. For the different stages of coronagraphic devices, we choose a diaphragm of 80% of the previous pupil diameter. All wavefronts errors are given for the mean wavelength of the Ks band (2.2 μm).